

Temporal Transductive Inference for Few-Shot Video Object Segmentation

Mennatullah Siam, Konstantinos G. Derpanis, Richard P. Wildes

Abstract—Few-shot video object segmentation (FS-VOS) aims at segmenting video frames using a few labelled examples of classes not seen during initial training. In this paper, we present a simple but effective temporal transductive inference (TTI) approach that leverages temporal consistency in the unlabelled video frames during few-shot inference. Key to our approach is the use of both global and local temporal constraints. The objective of the global constraint is to learn consistent linear classifiers for novel classes across the image sequence, whereas the local constraint enforces the proportion of foreground/background regions in each frame to be coherent across a local temporal window. These constraints act as spatiotemporal regularizers during the transductive inference to increase temporal coherence and reduce overfitting on the few-shot support set. Empirically, our model outperforms state-of-the-art meta-learning approaches in terms of mean intersection over union on YouTube-VIS by 2.8%. In addition, we introduce improved benchmarks that are exhaustively labelled (*i.e.* all object occurrences are labelled, unlike the currently available), and present a more realistic evaluation paradigm that targets data distribution shift between training and testing sets. Our empirical results and in-depth analysis confirm the added benefits of the proposed spatiotemporal regularizers to improve temporal coherence and overcome certain overfitting scenarios.

Index Terms—Few-shot Video Segmentation, Few-shot Segmentation, Few-shot learning, Video Object Segmentation, Transductive Inference, Temporal Consistency



1 INTRODUCTION

Few-shot object segmentation is concerned with segmenting novel classes in static images (*i.e.* the query set) aided with a few labelled images containing the novel classes (*i.e.* the support set) [1], [2], [3], [4], [5], [6], [7], [8]. Most approaches follow a meta-learning scheme that emulates the inference stage during training through sampling tasks of support and query sets (*i.e.* episodic training). Similar to few-shot object segmentation, few-shot video object segmentation (FS-VOS) segments objects in query videos with novel classes specified by a support set of images. Compared to few-shot segmentation, FS-VOS has received limited attention [9], [10].

Meta-learning has been widely explored in few-shot learning [2], [7], [11], [12]. Even so, recent work has pointed out issues in the applicability of meta-learning to the few-shot setting in realistic scenarios with domain shift [8], [13]. Transductive inference has emerged as a viable means to address some of these issues [8], [14], [15], [16], [17], [18]. Within the context of few-shot single image segmentation, recent work has shown that transductive inference can lead to surpassing the performance of non-transductive approaches [8]. In particular, superior performance came about via use of the prediction statistics of the unlabelled query imagery to regularize the learning of linear classifiers for the novel classes.

In general, transductive reasoning estimates the values of a particular set of examples for an unknown function, in contrast to inductive reasoning that learns to approximate

the general function and then uses the approximation to estimate the test examples [14]. In the few-shot setting, transductive inference uses the few-shot labelled support set along with the unlabelled query images to refine the learning of classifiers for novel classes [16] and classifies the query set as a whole at once [18]. Another important distinction is between transductive reasoning and semi-supervised learning, where the former uses the unlabelled query set and the later uses extra unlabelled data not necessarily confined to the query set [14], [18].

A naive extension of the transductive approach for *single image object* segmentation to *few-shot video object* segmentation learns a single classifier for each novel class on the entire video. However, we demonstrate in our experiments that regularization using the unlabelled query imagery fails when performed on the entire video. Instead, we have developed a novel temporal transductive inference (TTI) approach for few-shot video object segmentation. Key to our approach is the use of both global and local temporal constraints to learn a set of independent classifiers per-frame for the considered novel class. The global constraint enforces the per-frame classifiers to be globally consistent with a reference prototype (*i.e.* a class representative on the sequence level that is updated with every optimization iteration). The local constraint enforces the (framewise) foreground/background region proportions to be coherent over a temporal neighbourhood. Figure 1 provides an overview of our approach.

We also highlight two shortcomings with the evaluation protocol used in previous FS-VOS work [10]. First, the benchmark [10] does not provide exhaustively labelled masks, *i.e.* not all occurrences of a certain class are labelled. Second, it makes the strong assumption that the training and test sets are drawn from the same data distribution.

- M. Siam, K. Derpanis and R. Wildes are with the Department of Electrical Engineering and Computer Science, York University, Toronto, ON.
E-mail: {msiam, kostas, wildes}@eecs.yorku.ca

Manuscript received March 3, 2022;

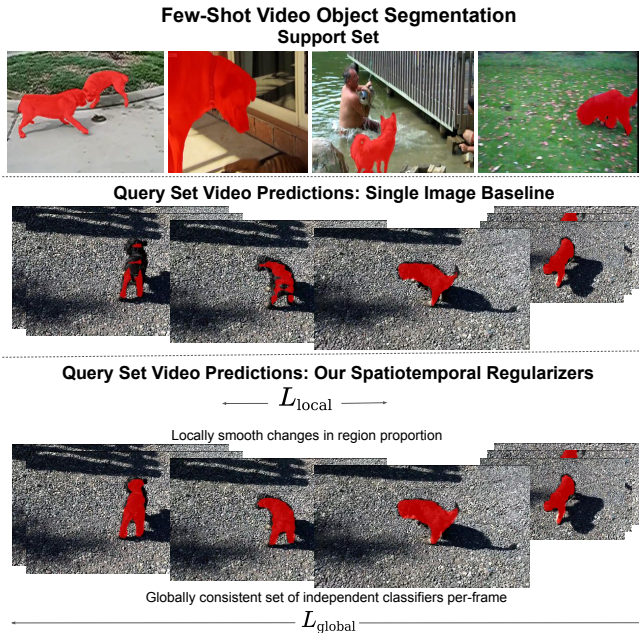


Fig. 1: Overview of our temporal transductive inference for FS-VOS. For each novel class, we learn an independent set of per-frame linear classifiers using the cross entropy loss on the support set and foreground/background region proportion regularization on the unlabelled query frames. We propose a set of spatiotemporal regularizers, including a global constraint that ensures a consistent set of linear classifiers on the video level, L_{global} , and a local constraint that ensures smooth changes for the region proportion across a local temporal window, L_{local} . Top: support set. Middle: query set predictions for our single image baseline. Bottom: query set predictions for our approach, demonstrating its superior temporal coherence in comparison to the baseline. The support set ground truth and query predictions are highlighted in red.

In realistic settings, there may be a significant data distribution shift between these sets. We provide illustrations of both these shortcomings in Sec. 5. To address these issues, we introduce a new benchmark that more closely aligns with the target task. Our benchmark uses the PASCAL-VOC dataset [19] as the training set and we re-purpose a densely labelled video semantic segmentation dataset, VSPW [20], as the test set. We refer to this cross-domain dataset as PASCAL-to-MiniVSPW. Further, we propose a score to assess the difficulty of the few-shot task for the baseline to demonstrate the benefit from our spatiotemporal regularizers in the most difficult scenarios.

Contributions. Overall, our contributions are fourfold. (i) We present a novel temporal transductive inference (TTI) approach that enforces global and local temporal consistency to regularize the learning of the classifiers with few-shot labelled examples. To the best of our knowledge, no previous research has used transductive fine-tuning for few-shot video segmentation. (ii) We introduce a novel keyframe-based fine-tuning of classifier weights during training. This approach allows the well segmented frames in a video to guide the training of other frames. Moreover, it avoids expensive on-line backbone fine-tuning [10], yet yields superior results. (iii) We improve the previously

proposed FS-VOS evaluation protocol by building an exhaustively labelled FS-VOS benchmark that operates cross-domain with data distribution shift, called PASCAL-to-MiniVSPW. We also present the MiniVSPW-to-MiniVSPW that does not operate cross-domain but has more sequences than PASCAL-to-MiniVSPW, while being exhaustively labelled. (iv) We propose a new score, k-shot stability, to assess the difficulty of the few-shot inference task for any approach and show that our spatiotemporal regularizers improve on the baseline in challenging scenarios. Moreover, we evaluate the temporal consistency of our predictions using a video consistency metric [20], which was lacking in previous work [10]. Our code and benchmarks are publicly available at https://github.com/MSiam/tti_fsvos.

2 RELATED WORK

Few-shot object segmentation. Most few-shot segmentation approaches are metric learning based. They mainly differ in how the support set is used to guide few-shot models, *e.g.* using a single vector representation from masked average pooling [2], [3], [21], co-attention [9], [22], multiscale feature enrichment [23] or graph neural networks [4]. Others explore a more powerful representation than what is afforded by a single prototype (*i.e.* class representative), *e.g.* use of part-aware prototypes [6] or prototype mixtures [7].

A major focus in the few-shot literature has been meta-learning. A major drawback of meta-learning approaches is their sensitivity to changes in the cardinality of the support set between training and testing [8], [24]. Transductive inference has been studied in the context of few-shot classification [15], [16], [25], [26], and was shown to have superior performance over meta-learning. Most closely related to our work is a single image classification approach that leveraged unlabelled query images to regularize fine-tuning of the final classifiers [8]. Notably, all these previous efforts focused on static images without considering temporal constraints available in video. We address this gap and propose a novel temporal transductive inference approach via use of spatiotemporal regularizers.

Video Segmentation (VS). Video segmentation trained on large-scale labelled datasets has been investigated heavily [27]. There are three main categories of approaches. (i) Automatic video object segmentation (VOS) segments objects that are visually and/or motion salient in an image sequence [28], [29]. (ii) Semi-automatic VOS relies on an initial labelled frame and subsequently tracks and segments the initialized objects throughout the sequence [30], [31], [32]. (iii) Semantic VS is concerned with segmenting a finite set of semantic categories that are learned during training [20], [33].

Both semi-automatic and automatic VOS are decidedly different than few-shot video segmentation. Semi-automatic VOS is provided with masks for the same objects in the sequence for subsequent tracking. FS-VOS is more challenging, as it uses a support set defined by imagery independent of the tracking video. The support set can be significantly different from the query video in terms of object properties (*e.g.* different dog breeds, color and texture) as well as different viewing conditions (*e.g.* viewpoint, lighting and

occlusion). Therefore, the latter can easily suffer from overfitting and needs to be equipped with specific strategies to generalize to novel classes from few labelled examples. As for automatic VOS, while it does not rely on an initial labelled frame, it can not be guided to segment certain semantic categories. In contrast, FS-VOS can exploit its support set to guide what classes are of specific interest. Overall, the FS-VOS task can be seen as the few-shot counterpart of video semantic segmentation that segments novel unseen classes beyond the finite set of classes used in training.

Temporal continuity constraints have proven useful in VOS [27]. Most closely related to the present work are the following examples. Semi-automatic VOS approaches have used unlabeled frames transductively to enforce temporal continuity [31], [32]. Earlier work on video semantic segmentation applied representation warping to fuse features from consecutive frames to ensure temporal consistency of the predictions in an inductive setting [33]. Unlike previous work, we focus on transductive inference for few-shot video segmentation.

Few-shot video object segmentation. Compared to video segmentation and few-shot segmentation with static imagery, there has been limited work on FS-VOS. Recent efforts focused on exploring attention [9], [10]. Co-attention conditioned on visual as well as semantic features was proposed and evaluated using a protocol that did not maintain the same support set on the entire sequence [9]. The other effort factorized full-rank many-to-many attention into two smaller components and proposed an evaluation protocol that used a single support set for the entire sequence [10]. All these approaches are meta-learning-based and thereby inherit the aforementioned meta-learning drawbacks. In contrast, we explore temporal transductive inference and show it is crucial in cross-domain scenarios. Additionally, we introduce two new benchmarks that address limitations in what was available previously [10].

3 PRELIMINARIES

3.1 Problem formulation

We formulate Few-Shot Video Object Segmentation (FS-VOS) as follows, *cf.* [10]. Let \mathcal{D}_{train} and \mathcal{D}_{test} be training and testing data, resp. For a dataset with C categories, split into O folds, each fold will have $\frac{C}{O}$ categories that comprise the novel test set, \mathcal{C}_{test} , while the remaining $C - \frac{C}{O}$ categories are used as base classes, \mathcal{C}_{train} , for training, with $\mathcal{C}_{train} \cap \mathcal{C}_{test} = \emptyset$. Classes in \mathcal{C}_{train} are represented with multiple instances in \mathcal{D}_{train} . For few-shot inference, we use episodic evaluation, where N_e tasks are sampled from \mathcal{D}_{test} with support and query set pairs $\{\mathcal{S}_i, \mathcal{Q}_i\}_{i=1}^{N_e}$. The support set in a one-way K -shot task has K image-label pairs $\mathcal{S} = \{X_k^{(s)}, M_k^{(s)}\}_{k=1}^K$, where superscript, $\cdot^{(s)}$, denotes support set and $M_k^{(s)}$ is a binary segmentation mask for a class of interest in \mathcal{C}_{test} . The image-label pairs $X_k, M_k \in \mathbb{R}^{W \times H \times 3}, \mathbb{R}^{W \times H}$, with $W \times H$ spatial dimensions. The few-shot models are then required to separate the class of interest from the background, hence the one-way evaluation. The query set has consecutive frames sampled from a video $\mathcal{Q} = \{X_t^{(q)}\}_{t=1}^{N_v}$, where superscript, $\cdot^{(q)}$, denotes query set and N_v is the number of frames.

3.2 Few-shot inference

In few-shot inference, the backbone model weights, θ , are taken as fixed and linear classifier weights, ω^l , and biases, b^l , are learned for the novel classes, where l stands for the optimization iteration. We are given a pair of support and query sets, $(\mathcal{S}, \mathcal{Q})$, as defined above. Inspired by weight imprinting methods, built on the relation between softmax classification and metric learning [5], [34], we consider the final classifier weights as class prototypes.

The extracted features, using the backbone, f_θ , from the support sets are defined as $F_k^{(s)} = f_\theta(X_k^{(s)})$ and normalized according to $\hat{F}_k^{(s)} = \frac{F_k^{(s)}}{\|F_k^{(s)}\|}$, and similarly for $F_t^{(q)}$. The novel class weights are initialized (imprinted) to the extracted prototype from the support set features according to

$$\omega^0 = \frac{1}{K} \sum_{k=1}^K \frac{\sum_{x,y} M_k^{(s)}(x,y) \hat{F}_k^{(s)}(x,y)}{\sum_{x,y} M_k^{(s)}(x,y)}, \quad (1)$$

where x, y are the spatial locations. For the sake of compactness of notation, throughout the rest of the paper we only use superscript $\cdot^{(s)}$ when denoting the support set, otherwise it is considered the query without the need for the additional superscript. Biases are initialized to the average of the initial foreground predictions on the query set [8], p_{fg}^0 , according to

$$b^0 = \frac{1}{WH} \sum_{x,y} p_{fg}^0(x,y). \quad (2)$$

We then estimate the per-pixel probabilities for belonging to the sampled class in the one-way task or background according to

$$p^l(x,y) = \begin{pmatrix} 1 - \sigma^l(x,y) \\ \sigma^l(x,y) \end{pmatrix}, \quad (3)$$

where $\sigma^l(x,y) = \text{sigmoid}(\tau(\langle F(x,y), \omega^l \rangle - b^l))$ with $\langle \cdot, \cdot \rangle$ denoting cosine similarity and τ a constant hyperparameter for scaling the output, *cf.* [8]. The formulation, Eq. 3, can be used for estimating both query and support set predictions. We use the notation p_{fg} to denote the foreground probability and similarly for the background probability, p_{bg} .

The linear classifier weights are trained using the cross entropy loss on the few-shot support set,

$$\mathbf{L}_{ce} = -\frac{1}{K} \sum_{k=1}^K \frac{1}{WH} \sum_{x,y} \hat{M}_k^{(s)}(x,y)^\top \log p_k^l(x,y), \quad (4)$$

where $\hat{M}_k^{(s)}$ is defined as the one-hot vector of the segmentation mask. By itself, *i.e.* without additional constraints, this formulation can lead to degenerate solutions. Previous single image object segmentation work has considered the foreground/background region proportion as a constraint; however, it is only applied to individual images [8]. We instead propose constraints that take temporal consistency into account, as natural for video object segmentation.

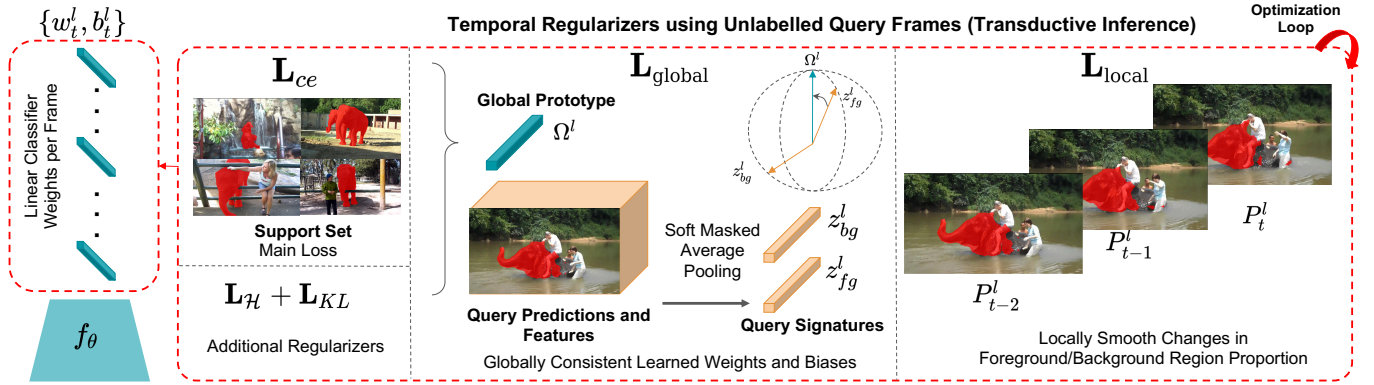


Fig. 2: Overview of our temporal transductive inference algorithm. Features are extracted from images using a backbone architecture, f_θ , from which linear classifier weights, w_t^l , and biases, b_t^l , are optimized for each frame, t , at each iteration, l . This optimization is performed using a cross entropy loss, \mathbf{L}_{ce} Eq. 4, with respect to the support set. Global consistency is enforced via a constraint, \mathbf{L}_{global} Eq. 7, that drives per query frame foreground signatures, z_{fg}^l Eq. 5, closer to the video global prototype, Ω_v^l Eq. 6, and further apart from the background signatures, z_{bg}^l Eq. 5 (visualized on a unit hypersphere). Local consistency is enforced via a constraint, \mathbf{L}_{local} Eq. 8, that drives foreground/background region proportions, P_t^l , to vary slowly within a local temporal window. Additional constraints, L_H and L_{KL} , increase prediction confidence and avoid focusing on too small regions using Eq. 9 and Eq. 10, resp.

4 TECHNICAL APPROACH

We present a novel temporal transductive inference approach to FS-VOS that exploits the temporal constraints inherent in unlabelled query video frames. In doing so, we introduce two main constraints (global and local) that contribute to the training loss by leveraging temporal relations in the query set. Global constraints encourage consistency to the learned prototype at the video sequence level. Local constraints encourage objects to undergo gradual scale changes within a local temporal window. An overview of our proposed algorithm is shown in Fig. 2. In the following subsections, we define our global as well as local constraints and the final learning scheme.

4.1 Global temporal consistency

Our global consistency constraint operates by encouraging frame-wise query signatures to be consistent with video-wise prototypes. The approach is motivated by theoretical results [17] that show the few-shot learning expected performance lower bound is correlated positively with the number of unlabelled query examples. Our use of the unlabelled examples is different, as we use pseudo-labels to compute query signatures and compute cosine similarity to per-video global prototype, while they used pseudo-labels to rectify the prototype per image; nevertheless, the underlying idea is similar.

Our approach operates as follows. We calculate foreground, z_{fg}^l , and background, z_{bg}^l , signatures at iteration l for individual query frames in the form of soft masked average pooling according to

$$z_{fg}^l = \frac{\sum_{x,y} p_{fg}^l(x,y) \hat{F}(x,y)}{\sum_{x,y} p_{fg}^l(x,y)}, \quad (5a)$$

$$z_{bg}^l = \frac{\sum_{x,y} p_{bg}^l(x,y) \hat{F}(x,y)}{\sum_{x,y} p_{bg}^l(x,y)}, \quad (5b)$$

resp., with $F = f_\theta(X)$, $\hat{F} = \frac{F}{\|F\|}$ and $p_{fg}^l(x,y), p_{bg}^l(x,y)$ calculated analogous to Eq. 3. These query foreground/background signatures act as a representative of what is classified as foreground or background based on the current set of weights.

For a sequence, v , with N_v frames, we calculate on the sequence level a global prototype

$$\Omega_v^l = \frac{1}{N_v} \sum_{t=1}^{N_v} \omega^l(t). \quad (6)$$

The prototype, Ω_v^l , is computed with every optimization iteration, l . We then use the signatures, Eq. 5, to regularize the learning for both weights and biases of novel classes to be consistent on the sequence level with the global prototype, Eq. 6. Thus, our temporal constraint is formulated as a transductive loss according to

$$\mathbf{L}_{global} = \frac{1}{N_v} \sum_{t=1}^{N_v} 1 - \langle \Omega_v^l, z_{fg}^l(t) \rangle + \frac{1}{N_v} \sum_{t=1}^{N_v} \max(0, \langle \Omega_v^l, z_{bg}^l(t) \rangle), \quad (7)$$

where $\langle \cdot, \cdot \rangle$ denotes cosine similarity. This global loss, Eq. 7, leads to maximizing the cosine similarity between the foreground signature of frame t , $z_{fg}^l(t)$, and the global prototype, Ω_v^l , while pushing it further away from the estimated background signature, $z_{bg}^l(t)$. We use $\max(0, \cdot)$ to ensure non-negative loss.

The optimization is repeated for several iterations, l . For each iteration, we recompute the global prototype, Ω_v^l , and the foreground/background signatures, z_{fg}^l, z_{bg}^l . This loss is motivated by the slowness principle, which entails

that important characteristics of the scene tend to change slower than the per-pixel individual measurements, *e.g.* [35]. In our case, since we seek to regularize the learning of weights and biases of the novel classes, we use the query predictions in a transductive manner to guide the extraction of foreground/background signatures per query frame. In that way, we drive the foreground signatures to be clustered together and further apart from the background signatures on the *sequence level*, instead of solely on consecutive frames. The learning thereby updates the linear classifier weights and biases while ensuring global consistency.

4.2 Local temporal coherence

Based on the assumption that objects undergo gradual scale changes within a local temporal window, we can expect the same for the foreground/background region proportion estimate, *i.e.* that it would change gradually within a local temporal window. Hence, we use the minimization of the rate of change for the region proportion estimate from consecutive query frames to enforce local temporal coherence. We compute the foreground/background region proportion estimate using label marginal distribution, $P = \frac{1}{WH} \sum_{x,y} p^l(x, y)$, with $p^l(x, y)$ calculated as above, Eq. 3.

Then, we estimate the rate of change for the label-marginal distribution on the query predictions within a local temporal window, N_w , using finite differences, leading to the loss

$$\mathbf{L}_{local} = \sum_{t=1}^{N_v} \sum_{i=1}^{N_w} |P(t) - P(t+i)|, \quad (8)$$

with t indexing successive video frames. This loss, Eq. 8, helps avoid erroneous predictions stemming from a poorly estimated prior marginal, P , in one of the frames.

4.3 Additional constraints

Following previous work on single image object segmentation with transductive inference [8], we incorporate two of their constraints into our approach. The first minimizes the entropy of the query predictions to increase its confidence. The second constrains foreground/background region proportion to avoid degenerate solutions.

Regions that are predicted with medium confidence are conserved through minimization of the prediction entropy. This constraint leads to the loss

$$\mathbf{L}_{\mathcal{H}} = -\frac{1}{WH} \sum_{x,y} p(x, y)^\top \log p(x, y). \quad (9)$$

Degenerate solutions, *e.g.* arising as emphasis on too small regions in an image in the query set, are further avoided by constraining foreground/background region proportions. In particular, the model predictions on the query are constrained to follow a prior distribution, P_ϕ , via the Kullback-Leibler (KL) divergence. This constraint is formulated as a loss

$$\mathbf{L}_{KL} = P^l \log \frac{P^l}{P_\phi}, \quad (10)$$

where $P_\phi = \frac{1}{WH} \sum_{x,y} p^l(x, y)$ is estimated from the label marginal distribution on the query predictions at $l = 0$,

then updated after L_ϕ iterations for a better estimate. While useful in avoiding focus on too small a foreground region, our preliminary experiments with the single image baseline indicated that this regularizer is sensitive to the prior label-marginal distribution, P_ϕ . In particular, it can lead to degenerate solutions if set to an erroneous prior due to early overfitting. We detail this scenario in the empirical results and show that our temporal regularizers reduce the effect of such problems. Since the baseline model minimizes this loss on a single image and has a different foreground/background region proportion estimate per query image, we perform it on every frame separately without temporal information.

4.4 Learning scheme

During training on the base classes, we follow the standard FS-VOS training paradigm with image-label pairs $\mathcal{D}_{train} = \{X_i, M_i\}_{i=1}^{N_{tr}}$ ([5], [8], [34]). The labels, M_i , are pixel-wise multi-class segmentation masks for the set of classes \mathcal{C}_{train} . Additionally, we use an auxiliary dense contrastive loss similar to previous work on the intermediate features when training the backbone on video datasets [36]. The loss is applied on temporally sampled frame pairs' features, $(\hat{F}_p(t), \hat{F}_{p+}(t+i))$, for frames $t, t+i$ and spatial position p , extracted before spatial pyramid pooling and normalized. This manipulation helps our model learn dense matching between frame pairs without relying solely on base class labels with the loss,

$$\mathbf{L}_{DCL} = -\log \frac{\exp(\hat{F}_p(t)^\top \hat{F}_{p+}(t+i)/\tau_{cl})}{\sum_{a \in A} \exp(\hat{F}_p(t)^\top \hat{F}_a(t+i)/\tau_{cl})}, \quad (11)$$

where $\hat{F}_p(t)$ is the anchor and $\hat{F}_{p+}(t+i)$ is the positive exemplar that is selected based on maximum cosine similarity to the anchor, the set A consists of all exemplars and τ_{cl} is the temperature hyperparameter.

During transductive inference, our final loss combines all terms defined above according to

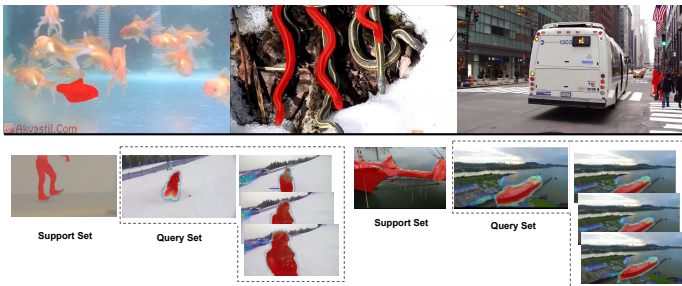
$$\mathbf{L} = \mathbf{L}_{ce} + \lambda_1 \mathbf{L}_{\mathcal{H}} + \lambda_2 \mathbf{L}_{KL} + \lambda_3 (\mathbf{L}_{global} + \mathbf{L}_{local}), \quad (12)$$

where λ_i are empirically determined weights. Linear classifier weights for the novel classes are optimized in two stages. (i) The weights are learned through the minimization of the final loss, Eq. 12, for L iterations. (ii) The weights are further optimized using the best predicted frame, t , which is referred to as the *keyframe* in the following. This frame is selected based on the highest cosine similarity between the foreground signature at frame t , $z_{fg}^L(t)$, according to Eq. 5, and the global prototype from Eq. 6. In particular, for a video, v , we define its keyframe as

$$v(t), \quad t = \underset{t}{\operatorname{argmax}} \langle z_{fg}^L(t), \Omega_v^L \rangle. \quad (13)$$

Keyframe pseudo-labels are constructed from their predictions following previous work [30]: A distance transform is used to select negative pixels far from the predicted positive pixels, while the remaining pixels are ignored to avoid erroneous labels. In this second stage only a cross entropy loss, analogous to Eq. 4, is used.

We provide an algorithmic summary in pseudocode detailing how the optimization process proceeds with our



YouTube-VIS-to-YouTube-VIS PASCAL-to-MiniVSPW

Fig. 3: Shortcomings in YouTube-VIS. Top: non-exhaustive labels in the annotations. Bottom: no distribution shift between the training and test sets, YouTube-VIS-to-YouTube-VIS, (left) *vs.* our proposed cross-domain dataset, PASCAL-to-MiniVSPW, (right). Ground truth masks and predictions are highlighted in red.

proposed spatiotemporal regularizers in Algorithm 1. The main transductive inference technique in the “TTI” function describes the first stage optimization process, which updates the final linear classifier weights and biases. Subsequently, in the second optimization stage (not illustrated in Algorithm 1), this process is followed by keyframe selection to perform additional fine-tuning of the weights learned in the previous stage.

5 FS-VOS BENCHMARK

5.1 Current FS-VOS shortcomings

The previously proposed FS-VOS protocol on YouTube-VIS [10] has two main shortcomings. First, YouTube-VIS is not exhaustively labelled, *i.e.* not all object occurrences in the sequence are labelled; see Fig. 3 (top). That limitation can cause issues for both training and few-shot inference, since the evaluation will be skewed to labelled instances only. Second, YouTube-VIS draws both its training and test sets from the same domain, *i.e.* same dataset without data distribution shift; see Fig. 3 (bottom). That design is inconsistent with more realistic scenarios where training data may well be drawn from a distinct distribution from the one where testing and ultimate deployment are likely to occur. For example, when adding video datasets with rare categories that are not present in currently available training data, cross-domain performance becomes critical.

5.2 Addressing YouTube-VIS shortcomings

In response to the shortcomings of YouTube-VIS, we introduce both the MiniVSPW-to-MiniVSPW and PASCAL-to-miniVSPW benchmarks. To remedy the first shortcoming (lack of exhaustive labeling) we employ the VSPW [20] dataset, which is exhaustively and densely labelled. VSPW also provides longer sequences than YouTube-VIS, with a higher annotation frame rate of 15 fps. These attributes make it more challenging and appealing to evaluate few-shot video object segmentation and leverage temporal consistency. We select a subset of VSPW that has categories overlapping with those of PASCAL-VOC. We specifically

Fold	Classes	# Images in Train	# Videos per Inf. Run
1	5	157858	610
2	5	153020	960
3	5	71813	261
4	5	158316	640

TABLE 1: MiniVSPW-to-MiniVSPW dataset statistics. The number of images used during training per fold, along with the number of sampled videos per run during the few-shot inference.

focus on PASCAL classes in both benchmarks that constitute things [37] classes and ignore stuff classes (*i.e.* wall, street, *etc.*). We consider stuff classes in our benchmark as *background*, because it can adversely affect the few-shot segmentation protocol otherwise. During training the established protocol in few-shot segmentation [10] is to label pixels belonging to the novel classes set as *background*. Therefore, if stuff classes are labelled separately from class *background* during training, they can contaminate the learning process. Our proposed protocol of selecting things classes only will prevent this problem. For MiniVSPW-to-MiniVSPW we split the classes into train, validation and test splits as detailed in Appendix A. Statistics for our benchmark in terms of number of images used for training and episodes (query videos) used in few-shot inference is shown in Table 1.

To remedy the second shortcoming (lack of cross-domain training and testing) we consider a more realistic cross-domain setting to simulate the domain shift that can occur between training and test data distributions in real-world applications. In particular, in PASCAL-to-MiniVSPW we use PASCAL-VOC 2012 [19] as the training dataset, while using a subset of VSPW as our test set. We create our subset by selecting only those classes in VSPW that have a corresponding PASCAL class. We also manually curate and filter sequences to resolve VSPW labelling ambiguities (*e.g.* mapping its category “bottle or cup” to “bottle” in PASCAL and filtering out sequences with “cup”). Following previous work [1], [8], PASCAL-VOC is split into four folds. Overall, PASCAL-to-MiniVSPW has 128 sequences with 8890 frames for the few-shot inference. We manually map categories between PASCAL-VOC and VSPW, as described in Appendix A.

Finally, we improve the protocol used in sampling the episodes on the YouTube-VIS benchmark. The previous protocol used for YouTube-VIS FS-VOS fixes the sampled support set for a novel class on all the query set videos belonging to that class in each run, and averages over five runs [10]. We call this protocol, *protocol I*. In contrast, we propose a random support set per query video instead of per class, since it allows for more random sampling and ensures more stable results. We call this new protocol, *protocol II*.

6 EMPIRICAL EVALUATION

6.1 Experiment design

Datasets and protocol. We evaluate on three datasets: (i) YouTube-VIS FS-VOS [10] to facilitate comparison to alternative approaches; (ii) our cross-domain benchmark PASCAL-to-MiniVSPW; (iii) our MiniVSPW-to-MiniVSPW

Algorithm 1 Temporal Transductive Inference (TTI) algorithm.

```

1: function FS-VOS INFERENCE(Input: Tasks =  $\{\mathcal{S}_i, \mathcal{Q}_i\}_{i=1}^{N_{te}}$ )
2:   for  $\mathcal{S} = \{X_k^{(s)}, M_k^{(s)}\}_{k=1}^K, \mathcal{Q} = \{X_t^{(q)}\}_{t=1}^{N_v}$  in Tasks do
3:      $F^{(q)} = f_\theta(X^{(q)}) \# [N_v \times C \times H \times W]$ 
4:      $F^{(s)} = f_\theta(X^{(s)}) \# [K \times C \times H \times W]$ 
5:     Normalize features to get  $\hat{F}^{(q)}, \hat{F}^{(s)}$ .
6:      $\{\omega^L, b^L\} = \text{TTI}(\hat{F}^{(q)}, \hat{F}^{(s)}, M^{(s)})$ .
7:     Compute  $p^L$  using  $\{\omega^L, b^L\}$  in Eq. 3.
8:   end for
9: end function
10: function TTI( $\hat{F}^{(q)}, \hat{F}^{(s)}, M^{(s)}$ )
11:   Compute initial label-marginal distribution per frame  $\{P^0(t)\}_{t=1}^{N_v}$ .
12:   Initialize  $\omega^0, b^0$  using Eq. 1 and 2, resp., for each frame set  $P_\phi(t) = P^0(t)$ .
13:   for Iteration  $l$  in  $\{1 \dots L\}$  do
14:     if  $l = L_\phi$  then
15:       Set  $P_\phi(t) = P^l(t)$ .
16:     end if
17:     if  $l < L_\phi$  then
18:        $\lambda_3 = 0, \lambda_1 = \lambda_2 = \frac{1}{K}$ 
19:     else
20:        $\lambda_3 = \frac{1}{K}$ 
21:        $\lambda_2 = \frac{1}{K} + 1$ 
22:       Compute  $\Omega_v^l$  according to Eq. 6, and compute  $z_{fg}^l(t), z_{bg}^l(t)$  per frame  $t$  using Eq. 5a and 5b, resp.
23:       Compute global constraint in Eq. 7.
24:       Compute label-marginal distributions per query frame prediction  $\{P^l(t)\}_{t=1}^{N_v}$ .
25:       Compute local constraint in Eq. 8.
26:     end if
27:     Compute additional constraints in Eq. 9 and 10.
28:     Compute the final loss  $\mathbf{L}$  using Eq. 12.
29:     Update per frame weights and biases  $\omega^l, b^l$  according to the gradients  $\frac{\partial \mathbf{L}}{\partial \omega^l}, \frac{\partial \mathbf{L}}{\partial b^l}$ .
30:   end for
31:   return  $\{\omega^L, b^L\}$ 
32: end function

```

benchmark. We choose as a baseline comparison algorithm a previous approach, RePRI, that made use of transductive inference, but without temporal modeling [8]. We also compare against several state-of-the-art approaches, listed in Table 2. We follow previous evaluations by reporting the mean Intersection over Union (mIoU) for one-way one-shot and five-shot evaluations, [8], [10]. We also use a video consistency metric, VC_w , to capture the consistency of estimates over a temporal window, w , [20]. This metric relies on a common area within the temporal window, where the semantic category does not change. It is calculated as the intersection of predictions, \hat{M} , in the common area ground truth, M , over the common area,

$$\text{VC}_w = \left(\bigcap_{i=1}^w \hat{M}_{t+i} \cap \bigcap_{i=1}^w M_{t+i} \right) / \left(\bigcap_{i=1}^w M_{t+i} \right). \quad (14)$$

We mostly report with temporal window, $w = 7$, but also systematically vary window size in Sec 6.4.2. Evaluation is performed over five runs and reporting the average, where in every run we sample 10000 episodes in the cross-domain paradigm [1]. In MiniVSPW-to-MiniVSPW we sample on average 600 episodes per fold as detailed in Sec. 5, while on YouTube-VIS we sample the same number of episodes as previous work [10]. For the sake of fair comparison between our approach and our baseline [8] on YouTube-VIS, we

run the two different transductive inference techniques on the exact same sampled support and query sets to avoid differences due to random sampling.

Model and training details. We follow the same architectural choices as our baseline [8] to facilitate comparison, where we build upon PSPNet [38] with the ResNet-50 [39] backbone. We specifically use ResNet-50 for fair comparison with [10]. We train the backbone on the base classes for a given fold using cross entropy, with 100 epochs on PASCAL-VOC and YouTube-VIS, while we use 10 epochs for MiniVSPW. For all common hyperparameters, we use the same as our baseline [8], we use SGD with a learning rate of 2.5×10^{-3} , momentum of 0.9, weight decay of 1×10^{-4} and cosine learning rate decay. Label smoothing is used with the smoothing parameter set to 0.1. Random flipping data augmentation also is used. We follow standard few-shot segmentation and few-shot video segmentation practices [1] of assigning the novel class objects that exist in training images to background.

Few-shot inference details. During transductive inference, we use a learning rate of 0.025 for $L = 50$ iterations; $L_\phi = 10$ and scaling factor $\tau = 20$. During inference on our introduced cross-domain benchmark, PASCAL-to-MiniVSPW, and MiniVSPW-to-MiniVSPW we resize images to 417×417 , while on YouTube-VIS we use 241×425 ,

Method	Query	Meta-Learning	mIoU					Δ_m	Δ_t	mVC ₇
			1	2	3	4	Mean			
PMMs [7]	Image	✓	32.9	61.1	56.8	55.9	51.7	-	-	-
PFENet [23]	Image	✓	37.8	64.4	56.3	56.4	53.7	-	-	-
PPNet [6]	Image	✓	45.5	63.8	60.4	58.9	57.1	-	-	-
DANet w/o OL [10]	Video	✓	41.5	64.8	61.3	61.4	57.2	0.1	-	-
DANet [10]	Video	✓	43.2	65.0	62.0	61.8	58.0	0.9	-	-
RePRI [8] (baseline)	Image	✗	45.8	68.6	59.3	64.2	59.5	2.4	-	58.1
Naive Temporal RePRI	Video	✗	36.6	62.0	50.2	55.2	51.0	-	-	-
TTI w/o DCL (ours)	Video	✗	47.5	69.5	60.5	63.8	60.3	3.2	0.8	62.7
TTI (ours)	Video	✗	48.2	69.0	62.8	63.1	60.8	3.7	1.3	63.6

TABLE 2: Comparison to the state of the art on YouTube-VIS with ResNet-50 backbone and five-shot support set following protocol I. Query Image: approaches that treat the query set as single images. Video: approaches that treat the video as a whole. Δ_m, Δ_t relative difference with respect to the best two single image baselines in meta-learning (PPNet [6]) and transductive inference (RePRI [8]), resp. mVC₇ mean video consistency on four folds with temporal window 7. We show DANet [10] with and without online learning (w/o OL). DCL: auxiliary dense contrastive loss used in our backbone training.

Method	mIoU					VC ₇				
	Fold 1	Fold 2	Fold 3	Fold 4	Mean	Fold 1	Fold 2	Fold 3	Fold 4	Mean
RepRI [8]	35.9	47.8	33.7	25.4	35.7	37.4	54.7	36.1	45.9	43.5
TTI (ours)	37.1	48.7	34.5	25.5	36.5	40.2	56.6	39.0	47.6	45.9

TABLE 3: PASCAL-to-MiniVSPW mIoU and video consistency, VC₇ Eq. 14, results with ResNet-50 backbone and one-shot one-way task.

Benchmark	Method	mIoU					VC ₇				
		Fold 1	Fold 2	Fold 3	Fold 4	Mean	Fold 1	Fold 2	Fold 3	Fold 4	Mean
P2M	RePRI [8]	38.5	53.1	40.0	31.7	40.8	39.8	51.4	29.1	29.2	37.4
	TTI	38.0	53.0	40.5	32.3	41.0	42.2	53.9	33.4	34.6	41.0
M2M	RePRI [8]	22.7	35.9	21.6	28.3	27.1	14.4	35.6	11.6	19.5	20.3
	TTI	25.2	37.1	25.0	29.6	29.2	18.6	40.2	15.9	22.9	24.4

TABLE 4: PASCAL-to-MiniVSPW (P2M) and MiniVSPW-to-MiniVSPW (M2M) benchmarks for five-shot one-way tasks.

Method	mIoU					VC ₇				
	Fold 1	Fold 2	Fold 3	Fold 4	Mean	Fold 1	Fold 2	Fold 3	Fold 4	Mean
RePRI [8] (baseline)	46.6	68.1	60.9	63	59.7	44.0	68.9	58.5	64.9	59.1
TTI (Local + Global)	47.2	68.8	61.4	63.5	60.2	45.8	70.4	60.4	66.4	60.8

TABLE 5: Comparison to our single image baseline on YouTube-VIS protocol II in terms of mIoU and Video Consistency VC₇. Our proposed protocol II ensures more stable results as it enforces random support set per query sequence.

as elsewhere [10]. During transductive inference our loss weights are initially set to $\lambda_1 = \frac{1}{K}$, $\lambda_2 = \frac{1}{K}$ and $\lambda_3 = 0$, as with our baseline (RePRI). After L_ϕ iterations, $\lambda_3 = \frac{1}{K}$, with K the number of shots, and λ_2 is increased by 1, again as with our baseline. These adjustments are made after L_ϕ iterations because the algorithm has converged to a better region proportion estimate to begin enforcing temporal coherence. The value of λ_1 remains constant across iterations. For the global consistency we use all the video frames when constructing the global prototype, and for the local temporal coherence, we use temporal window $N_w = 3$. In the cross domain paradigm in PASCAL-to-MiniVSPW, the model is trained on PASCAL-VOS base classes. Then during few-shot inference the support set is sampled from PASCAL-VOC for the novel classes, while query videos are sampled from MiniVSPW.

6.2 Comparison to state-of-the-art

Table 2 provides a comparison of our approach with respect to state-of-the-art FS-VOS alternatives. Both our baseline and proposed approach outperform the recent state-of-the-art meta-learning approach [10], which uses temporal information, by 1.5 – 2.8% mIoU. This result demonstrates that transductive inference can be sufficient for the few-shot task. Moreover, our approach improves over state-of-the-art single image approaches, the transductive inference baseline by $\Delta_t = 1.3\%$ and the meta-learning approach by $\Delta_m = 3.7\%$. Still, for fold four the transductive inference baseline, [8], outperforms our TTI approach. That particular result arises because fold four has some challenging classes that lead to over segmentation (e.g. “tennis racket”), which is exacerbated through temporal consistency processing. Our baseline does not suffer in this way on fold four, as it ignores temporal consistency. In contrast, when video consistency, Eq. 14, is considered we outperform our base-

Dataset	Global	Local	2^{nd} Stage Optimization	DCL	mIoU				
					Fold 1	Fold 2	Fold 3	Fold 4	Mean
PASCAL-to-MiniVSPW	✗	✗	✗	-	34.8	47.5	32.0	24.2	34.6
	✓	✗	✗	-	36.2	47.4	33.7	24.4	35.4
	✗	✓	✗	-	34.8	47.1	32.5	24.1	34.6
	✗	✗	Keyframe	-	34.6	47.0	32.0	24.1	34.4
	✓	✓	✗	-	36.6	47.5	34.0	24.4	35.6
	✓	✓	Keyframe	-	36.4	48.2	34.5	24.5	35.9
YouTube-VIS	✗	✗	✗	✗	45.8	68.6	59.3	64.2	59.5
	✓	✗	✗	✗	46.4	68.9	59.8	63.8	59.7
	✗	✓	✗	✗	45.9	68.9	59.4	64.4	59.7
	✗	✗	Keyframe	✗	47.3	68.7	60.3	63.2	59.9
	✗	✗	Random	✗	46.6	68.4	60.0	62.8	59.5
	✓	✓	✗	✗	46.6	69.2	60.0	64.1	60.0
	✓	✓	Keyframe	✗	47.5	69.5	60.5	63.8	60.3
	✗	✗	✗	✓	46.3	68.3	61.8	63.4	59.9
✓	✓	Keyframe	✓	48.2	69.0	62.8	63.1	60.8	

TABLE 6: Ablations showing mIoU on four folds for two benchmarks. Global and Local: global and local regularization, Eq. 7 and Eq. 8, resp. Keyframe: 2^{nd} stage optimization with keyframes, Eq. 13. Random: randomly selected frame. DCL: dense contrastive learning, Sec. 4.4.



Fig. 4: Qualitative results showing the temporal stability of our approach compared to the single image baseline on YouTube-VIS. Rows show different sequences and support sets. (a) Five-shot support set. (b) RePRI [8] (baseline). (c) TTI (ours). The support set ground truth and query predictions are highlighted in red.

line by 5.5%, which demonstrates the consistency of our predictions within a temporal window. Overall, these results demonstrate the value of including temporal modeling in transductive inference.

A simple approach for temporal transductive inference that uses a single set of weights for the novel classes for all frames is reported as “Naive Temporal RePRI”. It sums the losses from our baseline over all frames to update the weights, which degrades the results since the region proportion regularization is conducted with different priors. That flaw motivates our design that keeps separate sets of weights per frame.

Table 3 shows one-shot results of our approach with respect to the baseline on our new PASCAL-to-MiniVSPW dataset. Ours shows improvement of 0.8% on the mean over all folds, demonstrating the benefit from using temporal modeling in the presence of domain shift. The table also shows VC₇ as an additional confirmation that our approach exceeds the baseline in terms of video consistency with 2.4%. We use RePRI for comparison on this new benchmark as it is the strongest competitor on previous datasets in our evaluation. Figure 4 shows qualitative results to aid the argument that our results are temporally consistent.

We show quantitative results on the 5-shot PASCAL-to-MiniVSPW and MiniVSPW-to-MiniVSPW in Table 4. These results demonstrate that our approach consistently improves with respect to the baseline. Notably, in compar-

ison to the one-shot results, the five-shot results for video consistency generally decreases for both the baseline and our approach. This pattern can be attributed to scenarios where increased shot leads to under-segmentation, which is even aggravated more with taking the intersection over a sequence of frames between the predictions following the proposed metric [20]. We also demonstrate results for the YouTube-VIS improved protocol II in Table 5, which allows for a random support set with every sampled query set. These results show that even with the harder proposed protocol our method still outperforms with respect to the baseline.

Finally, we evaluate the run time of our TTI approach and find it to be 1.2 seconds/video, on average, executing on an A6000 Quadro GPU. For comparison, we consider the on-line learning approach that fine-tunes its ResNet-50 backbone at run time with 100 iterations [10] and find that it takes 85 seconds/video, on average, using the same hardware.

6.3 Ablation study

Table 6 shows the gains from our various modules for incorporating temporal information on both the PASCAL-to-MiniVSPW (with 1000 episodes) and YouTube-VIS. It is seen that the global module, Eq. 7, provides benefit on both datasets. In contrast, the local module, Eq. 8, does not impact the more challenging PASCAL-to-MiniVSPW, but

Fold	No L_{local}	$N_w = 3$	$N_w = 7$	$N_w = 11$
1	45.8	45.92	45.85	45.8
2	68.6	68.93	68.93	68.91
3	59.3	59.4	59.38	59.31
4	64.2	64.5	64.44	64.38
Mean	59.5	59.68	59.65	59.6

TABLE 7: Ablation study of the temporal window, N_w , used in the local loss showing (mIoU) on YouTube-VIS.

can combine with the global for overall improvement. Use of a second stage refinement with a keyframe, Eq. 13, as standalone also shows benefit on YouTube-VIS, but has little impact on PASCAL-to-MiniVSPW. When combined with the local and global modules, keyframe refinement leads to the best overall performance. This pattern of results is due to both the local and keyframe modules benefiting from good initial predictions, as provided by the global module, to either enforce local consistency or optimize on the keyframe. The table also compares second stage optimization using a randomly selected query frame *vs.* our proposed keyframe selection, Eq. 13, where it shows that our approach is superior.

Additionally, we consider improving the feature space via dense contrastive learning (DCL) [36] applied to temporally sampled frames. Two comparisons are given in Table 6 (YouTube-VOS): The penultimate and top rows compare models lacking spatiotemporal regularizers and keyframes with *vs.* without DCL; the bottom and third-from-bottom rows compare models including spatiotemporal regularizers and keyframes with *vs.* without DCL. In both comparisons, it is seen that DCL improves performance. Furthermore, in comparing the last row (our complete approach) and the penultimate row (with DCL, but without spatiotemporal regularizers and keyframes), we see that our proposed temporal transductive inference adds to the benefit of having stronger features from DCL alone. Thus, it confirms having good backbone features alone is not enough, and it is still crucial to have proper temporal constraints enforced during transductive inference to avoid overfitting. Finally, we ablate the temporal window used in the local loss, N_w , as shown in Table 7. It confirms that our results are stable with negligible decrease using larger windows. Nonetheless, we maintain using the best temporal window, $N_w = 3$, in all other experiments. In this set of experiments only the local regularizer was used during transductive fine-tuning to understand its effect without the global regularizer. A broader ablation study for our spatiotemporal regularizers and keyframe fine-tuning on all three different benchmarks including PASCAL-to-MiniVSPW (with 10000 episodes) is provided in Sec. 6.4.2.

6.4 Detailed Analysis

We hypothesize that the main reason behind improvement from our proposed spatiotemporal regularizers is that both the global loss, Eq. 7, and local loss, Eq. 8, reduce overfitting caused by the few-shot support set and produce temporally consistent predictions. To demonstrate the former, we propose a metric to capture the overfitting scenarios in Sec. 6.4.1. For the latter, we report the video consistency

metric with different temporal windows on the three benchmarks in Sec. 6.4.2.

6.4.1 Success and failure case analysis

All experiments in this section are conducted solely on the global and local losses without keyframe selection or contrastive loss. We make this choice to concentrate on the impact of the temporal transductive inference key components.

Overfitting is expected when learning the linear classifiers on few-shot labelled support sets, as it can lead to degenerate solutions. Our baseline includes regularization on a single frame to help overcome some of these issues, but that approach is sensitive to a prior on foreground/background region proportion [8]. A diagnostic of one form of overfitting is the accuracy for a five-shot ($K = 5$) support set, $\mathcal{S} = \{X_k^{(s)}, M_k^{(s)}\}_{k=1}^K$, being worse than the maximum accuracy obtained from using standalone examples, $(X_k^{(s)}, M_k^{(s)})$, from that set in a one-shot setting. This pattern indicates that certain examples in the support set confuse the model and negatively impact the query segmentation. Thus, let accuracy for five-shot and maximum accuracy across standalone examples be IoU_5 and $\max_k(\text{IoU}_1^k)$, resp. We calculate the K-shot stability score as, $\max_k(\text{IoU}_1^k) - \text{IoU}_5$; results are shown in Fig. 5.

Typically, accuracy should improve with increased shot size, but in certain cases it can lead to the opposite, as shown for our baseline in Fig. 5(a). While the majority of sequences benefit from additional support set examples, certain overfitting cases occur, where examples in the support set confuse the model rather than improve it. We are not the first to show that support set examples can affect the few-shot models differently [2]; however, we are the first to quantify and show its impact as an analysis for few-shot approaches. Fig. 5(a) shows that sequences suffering from this phenomenon decrease with our temporal regularizers in reference to the baseline.

We also show the mIoU gain or reduction from our approach with respect to the baseline as a function of K-shot stability in Fig. 5(b). The plot shows that our approach has a notable gain with respect to the baseline that consistently outweighs the cases where the opposite is seen. This result shows our temporal regularizers reducing failures in these overfitting scenarios over our baseline that does not take temporal constraints into account. Additionally, Fig. 5(d, e) shows qualitative examples of overfitting, with (d) providing predictions using the five-shot support set and (e) showing predictions from one-shot support set standalone. It is seen that examples where the support set is poorly representative of the query lead to overfitting and correspondingly bad predictions.

6.4.2 Temporal consistency analysis

We demonstrate in Fig. 6 the video consistency metric for our proposed approach with and without keyframe fine-tuning with different temporal windows as 3, 5, 7, 9, 11 to confirm the consistency of our results. As the temporal window increases the video consistency decreases, since it becomes more challenging to both our baseline and proposed approach (TTI). Interestingly, on all three benchmarks

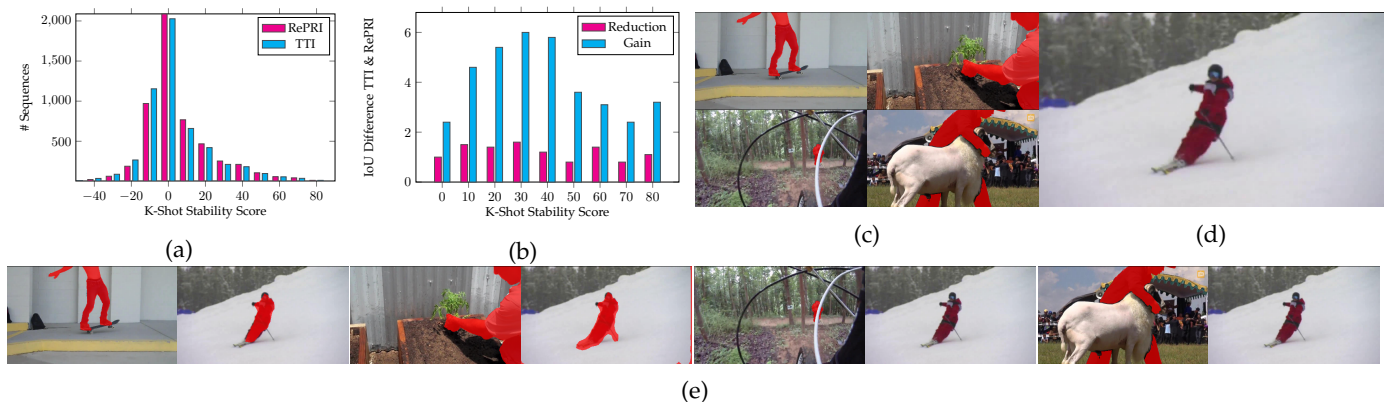


Fig. 5: Avoidance of overfitting through temporal coherence. (a) Histogram of K-shot stability scores, $\max_k(\text{IOU}_1^k) - \text{IOU}_5$, for the single image baseline [8] on YouTube-VIS Fold 1; high positive scores indicate overfitting due to the confusion from a few of the examples in the support set. (b) mIoU gains and reduction from our method with respect to the baseline [8]. (c, d, e) Example scenario where the linear classifiers are learned on a five-shot support set and compared to one-shot learning on every example standalone. (c) Five-shot support set. (d) Query prediction using five-shot. (e) Pairs of support set standalone examples and their corresponding query predictions.

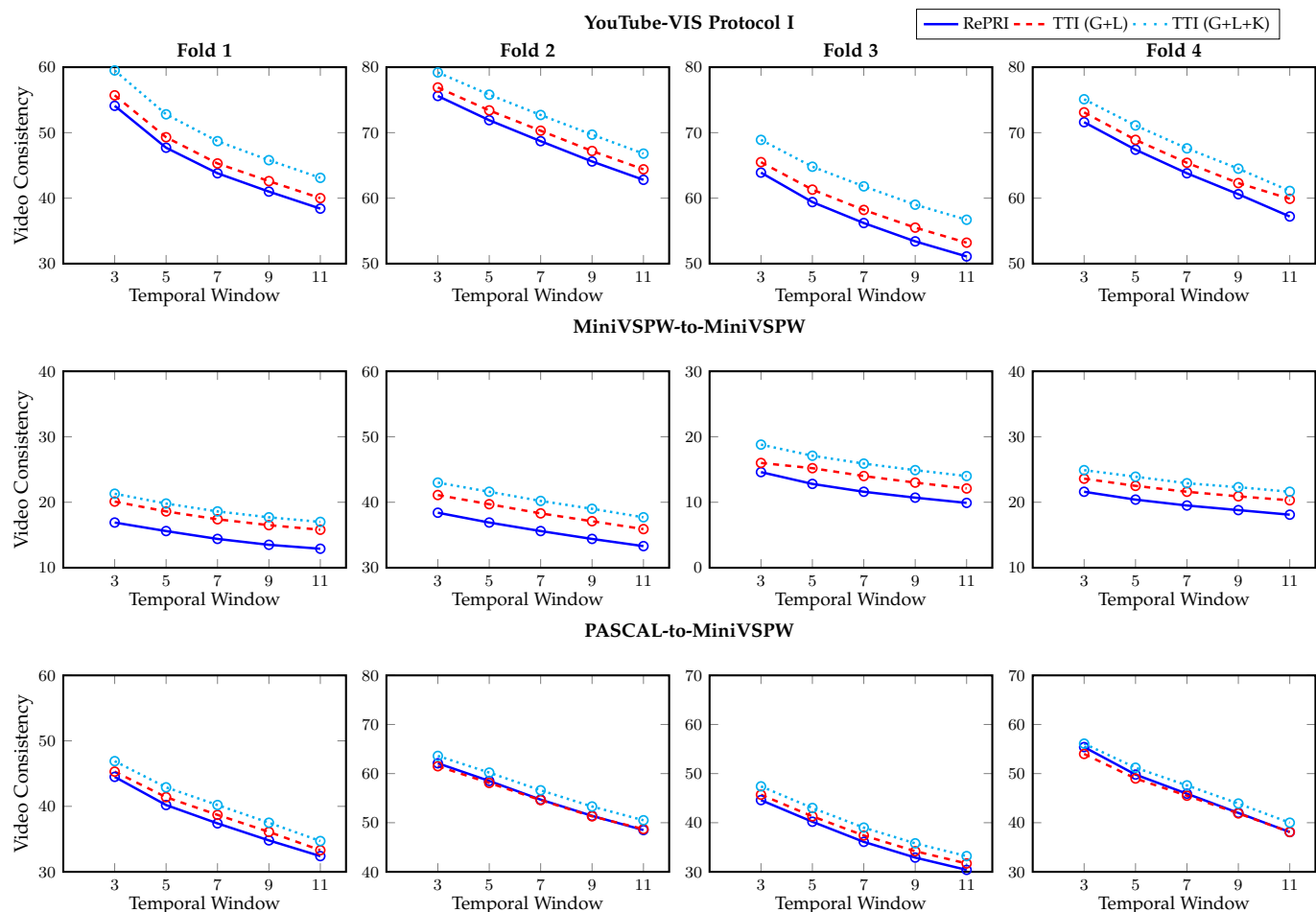


Fig. 6: Video consistency evaluated with different temporal window for our proposed TTI variants with respect to the single image baseline.

our final approach with spatiotemporal regularizers (*i.e.* global and local regularizers) and key frame fine-tuning is consistently improving with respect to the baseline on all four folds. Additionally, when looking only at the effect of our proposed spatiotemporal regularizers without keyframe

fine-tuning, we find it to outperform the baseline on most folds for all three benchmarks. This systematic evaluation on different benchmarks, folds and temporal windows further confirms the added benefit of temporally consistent predictions.

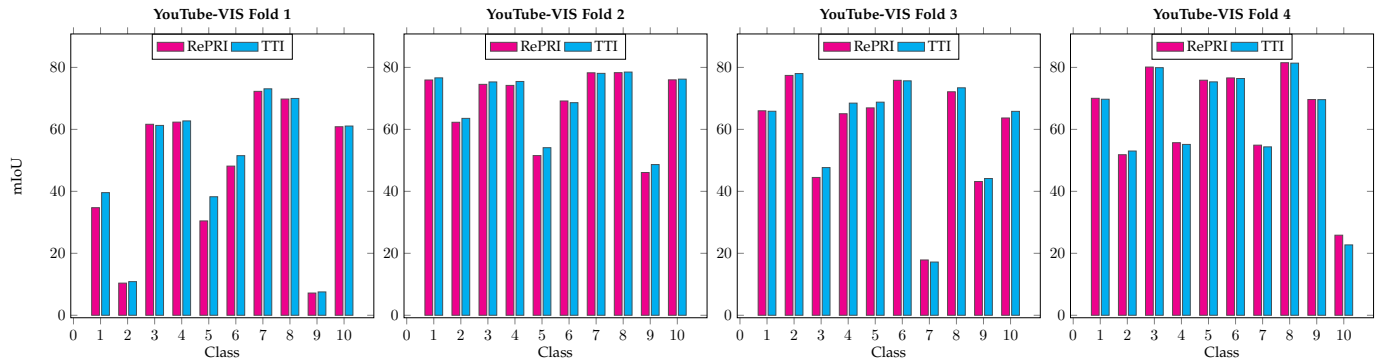


Fig. 7: Comparison between our approach without dense contrastive learning (TTI) *vs.* the single image baseline (RePRI [8]) in terms of intersection over union per class in a fold, evaluated for four folds each with ten classes on YouTube-VIS.

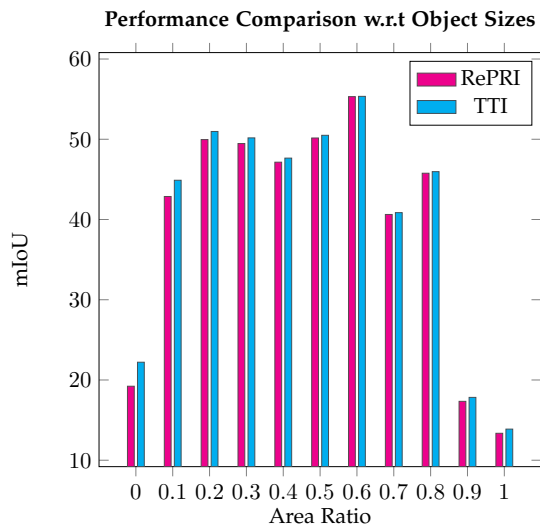


Fig. 8: Per-object-size IoU evaluation on YouTube-VIS comparing our proposed approach with respect to the baseline. TTI: our proposed method. RePRI [8]: our single image transductive inference baseline.

6.5 Class and object size analysis

We report results for mean intersection over union (IoU) averaged over all classes per fold, showing that our approach (TTI) improves on the single image baseline (RePRI [8]) in the mean over four folds. To provide a finer-grained comparison between TTI and RePRI, we compare per-class IoU and per-object-size IoU for our approach without dense contrastive learning (*w/o* DCL) *vs.* RePRI. Here, we concentrate on results without DCL to focus on the benefits offered by our spatiotemporal regularizers. Figure 7 shows the per-class IoU comparison for the four folds, each with ten classes and averaged over five runs. It is seen that multiple classes benefit from our spatiotemporal regularizers. Specifically, folds one, two and three show five classes in each fold to benefit from TTI over RePRI; indeed, certain classes reach up to 5% gain (*e.g.* first class in fold one). However, we suffer in the last fold from failure cases, which is reflected in degraded mIoU for fold four. These results are due to over segmentation that occurs with some challenging classes, as discussed in Sec. 6.2.

Additionally, we analyse the performance gain from our approach with respect to the baseline with varying object

sizes found in fold one in YouTube-VIS; see Fig. 8. We compute the area for the object using the ground truth masks and compute the area ratio as the ratio between the object *vs.* the entire image area. Then, we divide the area ratio into ten bins and compute the mean IoU for the objects whose sizes are within a bin. Interestingly, it is seen that TTI improves over RePRI, especially for the smallest (*e.g.* less than 50% area ratio) and largest (greater than 80% area ratio) objects, while the performance is more on par for intermediate size objects. For the smallest object sizes, the improvement is up to 3%.

7 CONCLUSION

We have presented a novel temporal transductive inference approach that uses global and local temporal constraints to improve the accuracy of FS-VOS. These constraints are enforced as losses during learning, with the global addressing weight consistency across a video and the local enforcing region proportion consistency. Our approach outperforms state-of-the-art alternatives on a standard benchmark. We also introduced two novel benchmarks. The first, PASCAL-to-MiniVSPW, better captures realistic domain shift scenarios than extant FS-VOS benchmarks. The second, MiniVSPW-to-MiniVSPW, addresses the problem with non-exhaustive annotations that were provided in YouTube-VIS by providing annotations that label all occurrences of each novel semantic category. Our approach also shows state-of-the-art performance on these new benchmarks.

APPENDIX A

FS-VOS BENCHMARKS

A.1 PASCAL-to-MiniVSPW benchmark

In this section we add more details about PASCAL-to-MiniVSPW benchmark. We found that there were only two PASCAL categories that lacked representatives in VSPW, “bird” and “sheep”, and they are not included in the evaluation protocol. Table 8 summarises our mapping between PASCAL and MiniVSPW.

A.2 MiniVSPW-to-MiniVSPW benchmark

We evaluate within the same domain for MiniVSPW to confirm the ability of our approach to improve with respect to the single image baseline. Since the MiniVSPW-to-MiniVSPW benchmark is not cross-domain, we use all the

Fold	PASCAL	MiniVSPW
Fold 1	aeroplane	airplane
	bicycle	bicycle
	boat	ship_or_boat
	bird	-
	bottle	bottle_or_cup
Fold 2	bus	bus
	car	car
	cat	cat
	chair	chair_or_seat
	cow	cattle
Fold 3	diningtable	table_or_desk
	dog	dog
	horse	horse
	motorbike	motorcycle
	person	person
Fold 4	pottedplant	flower_pot_or_vase
	sheep	-
	sofa	sofa
	train	train
	tvmonitor	screen_or_television

TABLE 8: PASCAL to MiniVSPW Mapping for the 20 PASCAL categories. Classes “bird” and “sheep” left out (denoted by -) as they do not have corresponding classes in VSPW.

sequences without the need to filter or curate sequences, which was required to avoid confusion when mapping the PASCAL to MiniVSPW classes. Additionally, we maintain the same splits of training and test classes, similar to PASCAL-5ⁱ [1], and use additional classes for the validation split as well as for replacing missing classes that are not available in MiniVSPW. We split the classes into train, validation and test splits as follows.

Fold 1:

- **Train:** bus, car, cat, chair_or_seat, cattle, table_or_desk, dog, horse, motorcycle, person, flower_pot_or_vase, sofa, train, screen_or_television, billboard_or_Bulletin_Board.
- **Validation:** blackboard, tent, truck, parasol_or_umbrella, cushion_or_carpet
- **Test:** airplane, bicycle, ship_or_boat, bottle_or_cup, book.

Fold 2:

- **Train:** airplane, bicycle, ship_or_boat, bottle_or_cup, cattle, table_or_desk, dog, horse, motorcycle, person, flower_pot_or_vase, sofa, train, screen_or_television, tent.
- **Validation:** billboard_or_Bulletin_Board, blackboard, book, parasol_or_umbrella, cushion_or_carpet.
- **Test:** bus, car, cat, chair_or_seat, truck.

Fold 3:

- **Train:** airplane, bicycle, ship_or_boat, bottle_or_cup, bus, car, cat, chair_or_seat, cattle, flower_pot_or_vase, sofa, train, screen_or_television, book, truck.
- **Validation:** blackboard, billboard_or_Bulletin_Board, parasol_or_umbrella, cushion_or_carpet, tent.
- **Test:** dog, horse, motorcycle, person, table_or_desk.

Fold 4:

- **Train:** airplane, bicycle, ship_or_boat, bottle_or_cup, bus, car, cat, chair_or_seat, table_or_desk, dog, horse, motorcycle, person, book, truck.
- **Validation:** blackboard, billboard_or_Bulletin_Board, parasol_or_umbrella, cushion_or_carpet, tent.
- **Test:** flower_pot_or_vase, sofa, train, screen_or_television, cattle.

A total of 482 sequences are used for testing and evaluation over all folds. Thus, MiniVSPW-to-MiniVSPW has more sequences than Pascal-to-MiniVSPW since we do not need manual filtering of the frames for ambiguous annotations as previously needed. It also provides a larger dataset for training than YouTube-VIS while maintaining exhaustive labels for all object occurrences.

REFERENCES

- [1] A. Shaban, Z. Bansal, Shrayand Liu, I. Essa, and B. Boots, “One-shot learning for semantic segmentation,” in *Proceedings of the British Machine Vision Conference*, 2017, pp. 167.1–167.13. **1, 6, 7, 13**
- [2] C. Zhang, G. Lin, F. Liu, R. Yao, and C. Shen, “CANet: Class-agnostic segmentation networks with iterative refinement and attentive few-shot learning,” in *Proceedings of the IEEE Conference on Computer Vision and Pattern Recognition*, 2019, pp. 5217–5226. **1, 2, 10**
- [3] K. Wang, J. H. Liew, Y. Zou, D. Zhou, and J. Feng, “PANet: Few-shot image semantic segmentation with prototype alignment,” in *Proceedings of the IEEE International Conference on Computer Vision*, 2019, pp. 9197–9206. **1, 2**
- [4] C. Zhang, G. Lin, F. Liu, J. Guo, Q. Wu, and R. Yao, “Pyramid graph networks with connection attentions for region-based one-shot semantic segmentation,” in *Proceedings of the IEEE International Conference on Computer Vision*, 2019, pp. 9587–9595. **1, 2**
- [5] M. Siam, B. N. Oreshkin, and M. Jagersand, “AMP: Adaptive masked proxies for few-shot segmentation,” in *Proceedings of the IEEE/CVF International Conference on Computer Vision*, 2019, pp. 5249–5258. **1, 3, 5**
- [6] Y. Liu, X. Zhang, S. Zhang, and X. He, “Part-aware prototype network for few-shot semantic segmentation,” in *Proceedings of the European Conference on Computer Vision*, 2020. **1, 2, 8**
- [7] B. Yang, C. Liu, B. Li, J. Jiao, and Q. Ye, “Prototype mixture models for few-shot semantic segmentation,” in *Proceedings of the European Conference on Computer Vision*, 2020, pp. 763–778. **1, 2, 8**
- [8] M. Boudiaf, H. Kervadec, Z. I. Masud, P. Piantanida, I. Ben Ayed, and J. Dolz, “Few-shot segmentation without meta-learning: A good transductive inference is all you need?” in *Proceedings of the IEEE/CVF Conference on Computer Vision and Pattern Recognition*, 2021, pp. 13979–13988. **1, 2, 3, 5, 6, 7, 8, 9, 10, 11, 12**
- [9] M. Siam, N. Doraiswamy, B. N. Oreshkin, H. Yao, and M. Jagersand, “Weakly supervised few-shot object segmentation using co-attention with visual and semantic embeddings,” in *Proceedings of the International Joint Conference on Artificial Intelligence*, 7 2020, pp. 860–867. **1, 2, 3**
- [10] H. Chen, H. Wu, N. Zhao, S. Ren, and S. He, “Delving deep into many-to-many attention for few-shot video object segmentation,” in *Proceedings of the IEEE/CVF Conference on Computer Vision and Pattern Recognition*, 2021, pp. 14040–14049. **1, 2, 3, 6, 7, 8, 9**
- [11] J. Snell, K. Swersky, and R. Zemel, “Prototypical networks for few-shot learning,” in *Advances in Neural Information Processing Systems*, 2017. **1**
- [12] O. Vinyals, C. Blundell, T. Lillicrap, K. Kavukcuoglu, and D. Wierstra, “Matching networks for one shot learning,” in *Advances in Neural Information Processing Systems*, vol. 29, 2016, pp. 3630–3638. **1**
- [13] W.-Y. Chen, Y.-C. Liu, Z. Kira, Y.-C. F. Wang, and J.-B. Huang, “A closer look at few-shot classification,” in *Proceedings of the International Conference on Learning Representations*, 2019. **1**
- [14] V. Vapnik, “Transductive inference and semi-supervised learning,” in *Semi-Supervised Learning*. MIT press, 2006, ch. 24, p. 454–472. **1**

- [15] A. Nichol, J. Achiam, and J. Schulman, "On first-order meta-learning algorithms," *arXiv preprint arXiv:1803.02999*, 2018. **1, 2**
- [16] G. S. Dhillon, P. Chaudhari, A. Ravichandran, and S. Soatto, "A baseline for few-shot image classification," in *Proceedings of the International Conference on Learning Representations*, 2020. **1, 2**
- [17] J. Liu, L. Song, and Y. Qin, "Prototype rectification for few-shot learning," in *Proceedings of the European Conference on Computer Vision*, 2020. **1, 4**
- [18] M. Boudiaf, I. Ziko, J. Rony, J. Dolz, P. Piantanida, and I. Ben Ayed, "Information maximization for few-shot learning," *Advances in Neural Information Processing Systems*, vol. 33, pp. 2445–2457, 2020. **1**
- [19] M. Everingham, L. Van Gool, C. K. Williams, J. Winn, and A. Zisserman, "The PASCAL visual object classes (VOC) challenge," *International Journal of Computer Vision*, vol. 88, no. 2, pp. 303–338, 2010. **2, 6**
- [20] J. Miao, Y. Wei, Y. Wu, C. Liang, G. Li, and Y. Yang, "VSPW: A large-scale dataset for video scene parsing in the wild," in *Proceedings of the IEEE/CVF Conference on Computer Vision and Pattern Recognition*, 2021, pp. 4133–4143. **2, 6, 7, 9**
- [21] K. Rakelly, E. Shelhamer, T. Darrell, A. Efros, and S. Levine, "Conditional networks for few-shot semantic segmentation," in *Proceedings of the IEEE International Conference on Machine Learning Workshops.*, 2018. **2**
- [22] X. Yang, B. Wang, K. Chen, X. Zhou, S. Yi, W. Ouyang, and L. Zhou, "BriNet: Towards bridging the intra-class and inter-class gaps in one-shot segmentation," in *Proceedings of the British Machine Vision Conference*, 2020. **2**
- [23] Z. Tian, H. Zhao, M. Shu, Z. Yang, R. Li, and J. Jia, "Prior guided feature enrichment network for few-shot segmentation," *IEEE Transactions on Pattern Analysis & Machine Intelligence*, 2020. **2, 8**
- [24] T. Cao, M. T. Law, and S. Fidler, "A theoretical analysis of the number of shots in few-shot learning," in *Proceedings of the International Conference on Learning Representations*, 2020. **2**
- [25] Y. Liu, J. Lee, M. Park, S. Kim, E. Yang, S. Hwang, and Y. Yang, "Learning to propagate labels: Transductive propagation network for few-shot learning," in *Proceedings of the International Conference on Learning Representations*, 2019. **2**
- [26] L. Qiao, Y. Shi, J. Li, Y. Wang, T. Huang, and Y. Tian, "Transductive episodic-wise adaptive metric for few-shot learning," in *Proceedings of the IEEE/CVF International Conference on Computer Vision*, 2019, pp. 3603–3612. **2**
- [27] W. Wang, T. Zhou, F. Porikli, D. Crandall, and L. Van Gool, "A survey on deep learning technique for video segmentation," *arXiv preprint arXiv:2107.01153*, 2021. **2, 3**
- [28] S. D. Jain, B. Xiong, and K. Grauman, "FusionSeg: Learning to combine motion and appearance for fully automatic segmentation of generic objects in videos," in *Proceedings of the IEEE Conference on Computer Vision and Pattern Recognition*, 2017, pp. 2117–2126. **2**
- [29] P. Tokmakov, K. Alahari, and C. Schmid, "Learning video object segmentation with visual memory," in *Proceedings of the IEEE International Conference on Computer Vision*, 2017, pp. 4481–4490. **2**
- [30] P. Voigtlaender and B. Leibe, "Online adaptation of convolutional neural networks for video object segmentation," in *Proceedings of the British Machine Vision Conference*, 2017. **2, 5**
- [31] Y. Zhang, Z. Wu, H. Peng, and S. Lin, "A transductive approach for video object segmentation," in *Proceedings of the IEEE/CVF Conference on Computer Vision and Pattern Recognition*, 2020, pp. 6947–6956. **2, 3**
- [32] Y. Mao, N. Wang, W. Zhou, and H. Li, "Joint inductive and transductive learning for video object segmentation," in *Proceedings of the IEEE/CVF International Conference on Computer Vision*, 2021. **2, 3**
- [33] R. Gadde, V. Jampani, and P. V. Gehler, "Semantic video CNNs through representation warping," in *Proceedings of the IEEE International Conference on Computer Vision*, 2017, pp. 4453–4462. **2, 3**
- [34] H. Qi, M. Brown, and D. G. Lowe, "Low-shot learning with imprinted weights," in *Proceedings of the IEEE Conference on Computer Vision and Pattern Recognition*, 2018, pp. 5822–5830. **3, 5**
- [35] H. Mobahi, R. Collobert, and J. Weston, "Deep learning from temporal coherence in video," in *Proceedings of the International Conference on Machine Learning*, 2009, pp. 737–744. **5**
- [36] X. Wang, R. Zhang, C. Shen, T. Kong, and L. Li, "Dense contrastive learning for self-supervised visual pre-training," in *Proceedings of the IEEE/CVF Conference on Computer Vision and Pattern Recognition*, 2021, pp. 3024–3033. **5, 10**
- [37] A. Kirillov, K. He, R. Girshick, C. Rother, and P. Dollár, "Panoptic segmentation," in *Proceedings of the IEEE/CVF Conference on Computer Vision and Pattern Recognition*, 2019, pp. 9404–9413. **6**
- [38] H. Zhao, J. Shi, X. Qi, X. Wang, and J. Jia, "Pyramid scene parsing network," in *Proceedings of the IEEE Conference on Computer Vision and Pattern Recognition*, 2017, pp. 2881–2890. **7**
- [39] K. He, X. Zhang, S. Ren, and J. Sun, "Deep residual learning for image recognition," in *Proceedings of the IEEE Conference on Computer Vision and Pattern Recognition*, 2016, pp. 770–778. **7**



Mennatullah Siam received B. Sc. degree from Computer Science in Ainshams University, Cairo in 2010, the MSc degree in Informatics from Nile University, Egypt in 2013 and the PhD degree from Computing Science department in University of Alberta, Edmonton, Canada in 2021. She is currently a postdoctoral researcher in the department of Electrical Engineering and Computer Sciences in York University, Toronto, Canada. She was a recipient of Alberta Innovates Foundations Technology and Verna Tate graduate scholarships, and is currently a recipient of VISTA postdoc fellowship. Her major fields of interest are few-shot segmentation, video object segmentation and few-shot video understanding.



Konstantinos G. Derpanis Kosta Derpanis received the Honours Bachelor of Science (BSc) degree in computer science with a Minor in mathematics from the University of Toronto, Canada, in 2000. He received the MSc (supervisors Prof. John Tsotsos and Prof. Richard Wildes) and PhD (supervisor Prof. Richard Wildes) degrees in computer science from York University, Canada, in 2003 and 2010, respectively. For his dissertation work, he received the Canadian Image Processing and Pattern Recognition Society (CIPPRS) Doctoral Dissertation Award 2010 Honourable Mention. Subsequently, he was a postdoctoral researcher in the GRASP Laboratory at the University of Pennsylvania under the supervision of Prof. Kostas Daniilidis. In 2012, he joined the Department of Computer Science at Ryerson University, Toronto, and later was promoted to Associate Professor with early tenure. In 2021, he joined the Department of Electrical Engineering and Computer Science at York University as an Associate Professor. He also serves as a visiting research scientist at Samsung Artificial Intelligence Center (SAIC), Toronto. His main research field of interest is computer vision with emphasis on motion analysis and human motion understanding, and related aspects in image processing and machine learning.



Richard P. Wildes Richard P. Wildes (Member, IEEE) received the PhD degree from the Massachusetts Institute of Technology in 1989. Subsequently, he joined Sarnoff Corporation in Princeton, New Jersey, as a Member of the Technical Staff in the Vision Technologies Lab. In 2001, he joined the Department of Electrical Engineering and Computer Science at York University, Toronto, where he is a Professor, a member of the Centre for Vision Research and a Tier I York Research Chair. He also is a visiting research scientist at Samsung Artificial Intelligence Center (SAIC), Toronto. Honours include receiving a Sarnoff Corporation Technical Achievement Award, the IEEE D.G. Fink Prize Paper Award and twice giving invited presentations to the US National Academy of Sciences. His main areas of research interest are computational vision, especially video understanding, and artificial intelligence.